Provided for non-commercial research and education use.
Not for reproduction, distribution or commercial use.

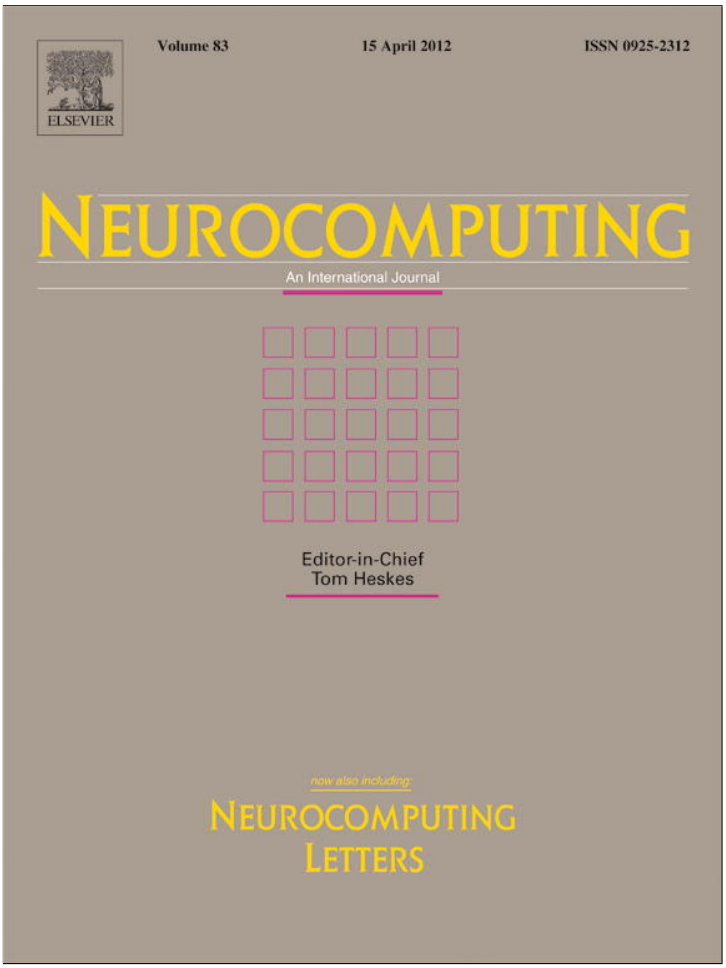

This article appeared in a journal published by Elsevier. The attached copy is furnished to the author for internal non-commercial research and education use, including for instruction at the authors institution and sharing with colleagues.

Other uses, including reproduction and distribution, or selling or licensing copies, or posting to personal, institutional or third party websites are prohibited.

In most cases authors are permitted to post their version of the article (e.g. in Word or Tex form) to their personal website or institutional repository. Authors requiring further information regarding Elsevier's archiving and manuscript policies are encouraged to visit:

http://www.elsevier.com/copyright

Author's personal copy

Neurocomputing 83 (2012) 146–157

Contents lists available at SciVerse ScienceDirect

Neurocomputing

journal homepage: www.elsevier.com/locate/neucom

Correlated firing and oscillations in spiking networks with global delayed inhibition

Jin-li Xie [a], Zhi-Jie Wang [a], Andre Longtin [b,*]

[a] College of Information Science and Technology, Donghua University, Shanghai 201620, China
[b] Department of Physics and Center for Neural Dynamics, University of Ottawa, 150 Louis Pasteur, Ottawa, Ont., Canada K1N 6N5

ARTICLE INFO

Article history:
Received 24 June 2011
Received in revised form
8 October 2011
Accepted 5 December 2011
Communicated by T. Heskes
Available online 27 December 2011

Keywords:
Electric fish
Global feedback
Gamma oscillations
Noise
Correlations

ABSTRACT

In feed-forward networks, output pairwise correlations can increase with firing rate. Here, we study correlations between sensory neurons with global inhibitory feedback and cross-correlated external inputs. The average pairwise correlation coefficient is computed from simulations of a network of noisy leaky integrate-and-fire neurons with delayed spike-driven feedback. We focus on the relation between the correlation and the feedback strength. This relation is monotonically increasing when the common noise is frozen, and non-monotonic when it varies across trials. In both cases, beyond a certain feedback strength, the increase in correlation mirrors the emergence of asynchronous network oscillations quantified by the sharpness ("coherence") of the peak in the spike train power spectral density. Our results suggest that pairwise correlations are strongly controlled by feedback via the interplay of mean firing rate and oscillatory activity. For frozen common noise, correlations in fact remain near zero up until oscillatory activity is sufficiently coherent. These results are found in both sub- and supra-threshold dynamic regimes, for low and moderate internal noise levels, as well as for a heterogeneous distribution of feedback gains or firing thresholds.

© 2012 Elsevier B.V. All rights reserved.

1. Introduction

Correlated neural activity has been observed in a variety of functional areas, including those involved in attention [40], audition [12], vision [10], olfaction [14], electrosensation [6] and motor control [34]. The properties of such activity are suspected to be critical for sensory and cortical processing [7,16,11]. The mechanisms underlying pairwise correlations, including the influence of connectivity, continues to attract the attention of theorists and computational neuroscientists (see e.g. [15,28,7,25,42,41,44,45]).

The interpretation of correlations is difficult, especially in large networks [43]. Precise measurements of correlations, in conjunction with modeling studies, are key to understanding their sources and roles. Correlations are often minute [11], and active de-correlating mechanisms may be at work [41]. It is also important to understand the correlating effect of specific dynamical states such as network oscillatory states [4,8,28,18,14,31,37]. Correlations have been described in non-delayed recurrent networks with mixtures of excitation and inhibition [15,25,41], including balanced states [19] or chaotic states with temporal variability that is stabilized by inhibitory feedback [17].

Recent work has further emphasized the role of shared stimulus inputs [14,13,47,21] and background activity [37]. Other efforts have quantified the range of temporal scales over which correlations occur [42], as well as the spatial extent of correlations [26,23]. For example, fast correlations over a small region appear consistent with common input, while slow correlations over broad regions seem to be associated with feedback [2,24,43].

It is generally known that inhibition can control high frequency [30,18] as well as spontaneous activity in cortex [1]. On the other hand gamma oscillations, thought to be fundamental for transmitting information [3], rely on inhibitory interneurons [48,5,33], and arise from oscillatory, synchronized firings of these interneurons onto pyramidal cells [4]. In the electrosensory system, oscillations and inhibition are linked via global delayed inhibitory feedback [8,9,28,31], and will be our focus here. Further, output pairwise correlations in feed-forward circuits generally increase with firing rate [7,10,36]. This is so when input correlations are not too strong, otherwise the output correlation becomes independent of firing rate [45]. This suggests that inhibition could on the one hand decrease correlations by suppressing firing; on the other hand, it is a form of coupling which can potentially correlate firings, especially if it induces oscillations [14,32].

Thus the question of how inhibition alone and oscillations interact to shape correlations in spiking networks is open, and of special interest for sensory systems. Here we investigate correlations in a network of excitatory neurons. The network receives correlated external input and can exhibit oscillations, and the cells inhibit each other via all-to-all delayed inhibition.

* Corresponding author.
E-mail address: alongtin@uottawa.ca (A. Longtin).

0925-2312/$ - see front matter © 2012 Elsevier B.V. All rights reserved.
doi:10.1016/j.neucom.2011.12.004

Author's personal copy

This backbone architecture is directly inspired by the electric sense [8] and the olfactory sense to a lesser extent [14]. Correlation is assessed by a measure of linear cross-correlation between spike trains [39,2,24,7,44]. We quantify network oscillations by the coherence of the associated spectral peak (peak height divided by relative width: [38,27]), and evaluate the influence of feedback strength on this coherence, mean firing rate and correlation. Finally, since parameter heterogeneity often reduces correlations [4,3], we further investigate the role of heterogeneity in our model.

Section 2 presents the model under study and the numerical methods to estimate the correlation. Section 3 presents our main results on how feedback influences correlation. Section 4 studies the correlative effect of emergent oscillations using spectral methods. The effect of heterogeneity is the focus of Section 5. A discussion and outlook onto future work follow in Section 6.

2. Model and numerical methods

We use a network of leaky integrate-and-fire (LIF) neuron models to analyze the pairwise correlations of spiking activities. The model comes from studies of the lateral line lobe of weakly electric fish, where principal cells are connected foremost through feedback [8,9,28]. These principal cells are also known as pyramidal cells, and provide the main output of this lobe structure. This model describes the dynamics of the membrane potential of neuron i as follows:

$$C\frac{dv_i}{dt} = -g_l v_i + \mu_E + \eta_i(t) + S_i(t) - I_G \tag{1}$$

where v and S are the membrane potential and input current, respectively. The capacitance C and the leak conductance g_l are set to one. The last term I_G represents feedback (see below). Also, μ_E denotes the base current (referred hereafter as the bias), and $\eta_i(t)$ is an internal zero-mean Gaussian white noise of intensity D_E that represents synaptic and channel noise in-vivo. Time is measured in units of the membrane time constant, which in the weakly electric fish is around 6 ms [8,9]. Every time the potential reaches the fixed firing threshold v_T, the neuron is said to fire, and the voltage is immediately reset to a value v_R where it remains for the absolute refractory time τ_R equal to 1 membrane time constant (an after-hyperpolarizing current makes this refractory period rather long). The output spike train of the LIF model is obtained by collecting the instants of threshold crossing and modeling the associated spikes as δ-functions:

$$y(t) = \sum_j \delta(t - t_j), \tag{2}$$

where the t_j are the successive firing times. The structure of the network model, shown in Fig. 1, includes N excitatory LIF neurons, which all provide excitatory input to an inhibitory LIF neuron [31]. The inhibitory feedback response from this neuron reaches all the excitatory neurons in layer 1 after a fixed time delay with respect to when it left the excitatory cells in layer 1, mimicking finite axonal transmission time.

Each excitatory neuron (numerated circles in Fig. 1) receives an input $S_i(t)$ from a sensory neuron, which for simplicity just relays the physical external stimulus. It is composed of the following components (motivated by work on natural inputs in the electric sense—see [9,28]):

$$S_i(t) = \sigma\left[\sqrt{1-c}\,\xi_i(t) + \sqrt{c}\,\xi_c(t)\right] \tag{3}$$

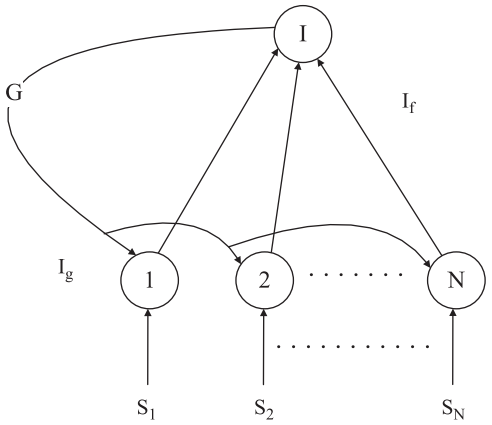

Fig. 1. Network model. A population of sensory neurons S sends afferent fibers to a layer of principle cells in layer 1 (circles labeled 1 to N). These principle cells send excitatory projections to a postsynaptic target. This could be another layer in the same or different nucleus, and is modeled here by a single neuron, which in turn sends inhibitory feedback to all the principle cells.

where $\xi_i(t)$ is a noise specific to each neuron (i.e. the $\xi_i(t)$ are independent across neurons) and represents local fluctuations in the physical environment, caused e.g. by small objects, prey or movement. The term $\xi_c(t)$ is a common noise, independent from all the other $\xi_i(t)$ and shared by all neurons. It mimics global stimuli such as large objects, or other fish in Doiron et al. [8,9]. These latter two noises are here made more realistic by being band-limited as in experiments ([9,7])—in contrast to the internal noise that is considered Gaussian white noise. The individual noise could have been lumped with the internal noise, but we chose it separate for our work given their different physical source. The external noises consist of two Gaussian low-pass filtered (0–150 Hz, eight-order Butterworth filter) noise processes of unit variance. They are scaled by the input correlation coefficient c to determine the degree of shared input of all the excitatory neurons: $c=0$ means the neurons have no shared external noise, while $c=1$ means the external noise is completely shared by the neurons. In this form, varying the input correlation does not change the total intensity of the external input noise. We set $c=0.6$ throughout our study, but also quote results for a lower value.

The last term in Eq. (1) represents the inhibitory feedback generated by the inhibitory neuron, calculated by the convolution of a delayed α function and the spike train y_I of the inhibitory neuron:

$$I_G(t) = G\int_{\tau_D}^{\infty} \alpha(\tau) y_I(t-\tau)\,d\tau \tag{4}$$

with

$$\alpha(t) = \frac{t-\tau_D}{\tau_S^2}\exp\left[-\frac{t-\tau_D}{\tau_S}\right]. \tag{5}$$

The feedback strength in Eq. (4) (referred hereafter as feedback gain G) is set to be positive, but the inhibitory current in Eq. (4) appears with a negative sign in Eq. (1). Increasing the gain G thus means a stronger inhibitory feedback current. Here τ_D is half the transmission delay around the feedback loop, and τ_S is the time constant of synaptic responses. The output of an LIF neuron provides here the inhibitory feedback to the excitatory neurons [31], rather than the sum of spike trains from the excitatory neurons themselves [8,28]. As shown in Marinazzo et al. [31], this does not qualitatively affect the behavior of the excitatory neurons, yet provides a first step towards exploring the frequency response of the feedback, and in particular its plasticity. The output of excitatory neurons convoluted with another delayed α

Author's personal copy

function provides only part of the input to the inhibitory neuron, as it also has a constant base current $\mu_I=0.9$ and internal Gaussian white noise $\eta(t)$ with intensity $D_I=0.112$:

$$I_f=\mu_I+\eta(t)+\int_{\tau_D}^{\infty}\alpha(\tau)\sum_{i=1}^{N}y_i(t-\tau)d\tau. \tag{6}$$

With this network model, we can easily change the dynamic regime of the excitatory neurons by setting the values of μ_E and D_E above or below the firing threshold v_T of the LIF neurons in layer 1. For $\mu_E<v_T$, the neurons are silent in the joint absence of internal noise, external noise and feedback. This is referred to as the sub-threshold regime. For this case, increasing internal noise significantly shortens the mean firing period. The other dynamic regime of interest is the supra-threshold regime for $\mu_E>v_T$, where deterministic firing occurs even without internal noise, external noise and feedback. For simplicity, our investigation of the correlated activity of the excitatory neurons will be carried out for only two different values of the intensity of the internal noise, $D_E>v_T$ and $D_E<v_T$. This will be done in both the sub-threshold and supra-threshold regimes.

The pairwise spike correlation measures the relative spike timing of two neurons. To compute the pairwise spike correlations, we use the spike train cross-correlogram (*CCG*) [39,2,24,6] rather than the spike count over a small counting window [7]. It is defined as

$$CCG_{ij}(\tau)=\frac{\sum_{k=1}^{M}\sum_{t=0}^{L}y_i^k(t)y_j^k(t+\tau)}{M(L-|\tau|)\sqrt{\lambda_i\lambda_j}}, \tag{7}$$

where M is the number of trials or realizations, L is the duration of every trial, and λ_i and λ_j are the firing rates of neurons i and j, respectively. Spike trains of two neurons y_i^k and y_j^k are defined as in Eq. (2). Here, we represent y_i^k and y_j^k as binary time series with 1 ms resolution. In each bin, $y_i^k=1$ ($y_j^k=1$) if neuron i (j) on trial k fires one or more spikes during this millisecond; otherwise, $y_i^k=0$ ($y_j^k=0$). The term $L-|\tau|$ is used to correct for the degree of overlap as a function of the discrete time lag τ of the two spike trains. Due to the division of the correlation function by the geometric mean spike rate $\sqrt{\lambda_i\lambda_j}$, *CCG* ends up with units of coincidences per spike.

The auto-correlograms (*ACG*) of the neurons, used below to normalize the cross-correlograms, are calculated similarly as the *CCG*, but by letting $i=j$:

$$ACG_{jj}(\tau)=\frac{\sum_{k=1}^{M}\sum_{t=0}^{L}y_j^k(t)y_j^k(t+\tau)}{M(L-|\tau|)\sqrt{\lambda_j\lambda_j}}. \tag{8}$$

Here we need to distinguish between correlations attributable to the stimulus (signal correlations) from those that are not (noise correlations). A standard technique to perform this distinction is to correct all *CCGs* and *ACGs* by subtracting the shift predictor *SPT*. This factor is based on the same normalization as above but calculated with different trials, k and k' [39]:

$$SPT_{ij}(\tau)=\frac{\sum_{k=1}^{M}\sum_{t=0}^{L}y_i^k(t)y_j^{k'}(t+\tau)}{M(L-|\tau|)\sqrt{\lambda_i\lambda_j}}, \tag{9}$$

where $k'=k+1(k<M)$ or $k'=1(k=M)$. By subtracting the shift predictor, the method to estimate the correlation coefficient is very similar to that in other studies [39,2,24,6]; a slight difference here is that the outer sum extends from 1 to M (instead of $M-1$). The pairwise spike correlation of the two neurons i and j is estimated by the ratio of the area of the *CCG* within a certain range of lags defining a window T to the geometric mean area of the *ACG* over the same window:

$$C_{ij}(T)=\frac{\sum_{\tau=-T}^{T}CCG_{ij}(\tau)-\sum_{\tau=-T}^{T}SPT_{ij}(\tau)}{\sqrt{\left[\sum_{\tau=-T}^{T}ACG_{ii}(\tau)-\sum_{\tau=-T}^{T}SPT_{ii}(\tau)\right]\left[\sum_{\tau=-T}^{T}ACG_{jj}(\tau)-\sum_{\tau=-T}^{T}SPT_{jj}(\tau)\right]}}. \tag{10}$$

When T is large enough, C_{ij} saturates to a steady state value $\bar{C}_{ij}$. Here C_{ij} is defined as the pairwise correlation coefficient of neurons i and j. Finally, the correlation coefficient *Cor* of the network reported below is obtained by averaging the pairwise correlation coefficients over all pairs of excitatory neurons:

$$Cor=\frac{1}{N(N-1)/2}\sum_{i=1}^{N}\sum_{j=i+1}^{N}C_{ij}. \tag{11}$$

In order to calculate *Cor* for each parameter set, $M=100$ trials, each with time duration $L=11$ s, were simulated. We remove the first 1 s of each trial to avoid the influence of the initial transient response. *CCGs* and *ACGs* are computed individually for each group, then corrected by the shift predictor. The shared input $\xi_c(t)$ in Eq. (3) is either (1) fixed for all trials, or (2) different for every trial. We report on results for both cases. The parameter values chosen in our work are: $N=100$, $\tau_D=4$ ms, $\tau_S=0.5$ ms, $\sigma=0.2$, $T=100$ ms, $v_T=1, v_R=0, \tau_R=1$. Eq. (1) is integrated using an Euler–Maruyama scheme with a time step of 5×10^{-5} s.

3. Pairwise correlation results

We first illustrate the behavior of our model in open-loop ($G=0$) and for two non-zero feedback strengths. Fig. 2 shows the raster plots, the population averaged firing rate, the feedback current, and the membrane potential for one randomly chosen neuron. The plot shows a drop in firing rate, and a clear progression from spike trains with little structure to network oscillations, with firings more phase locked to this oscillation. Fig. 3 shows the structure of the cross-correlograms at different values of G for the case of frozen common noise. The left panels show the shift predictors, and the right panels the *CCG* after subtraction of the SPT. We note that a peak appears around lag zero. It increases with feedback gain, which reflects increasing pairwise correlations. The delayed feedback is responsible for the bumps in the *CCG*, whose magnitudes increase with G. These *CCGs* are similar to the *ACGs* except at very short lags, as in [28]. Note that, in contrast, the SPT's for the case where the common noise varies across trials are flat (not shown).

We further note that the *CCGs* are symmetric. This is expected because each neuron in the network has identical parameters and receives the same delayed inhibitory feedback. This global feedback thus has the same effect on the firing activity of all the excitatory neurons. *CCG's* may show some asymmetry for particular neuron pairs if the neurons are different (as in Section 5), because their firing rates will be different [45]; this will be averaged out to a large extent when *Cor* is computed as an average over neuron pairs.

We now explore the relationship between the correlation coefficient of the network and the inhibitory feedback gain. We focus for now on the case where the common noise is frozen across trials. Later we show results when the common noise varies across trials. First, a sub-threshold base current $\mu_E=0.9$ with low internal noise $D_E=0.112$ is chosen. In this case, spikes are solely induced by noise (internal and external). As shown in Fig. 4 (top), *Cor* first remains constant near zero for small values of the feedback strength G, but later rises after G exceeds some value. Afterwards, a stable and relatively high level of pairwise correlation is maintained with further increases in G. In the supra-threshold regime, where μ_E is raised to $\mu_E=1.2$, the curve of *Cor* vs

Author's personal copy

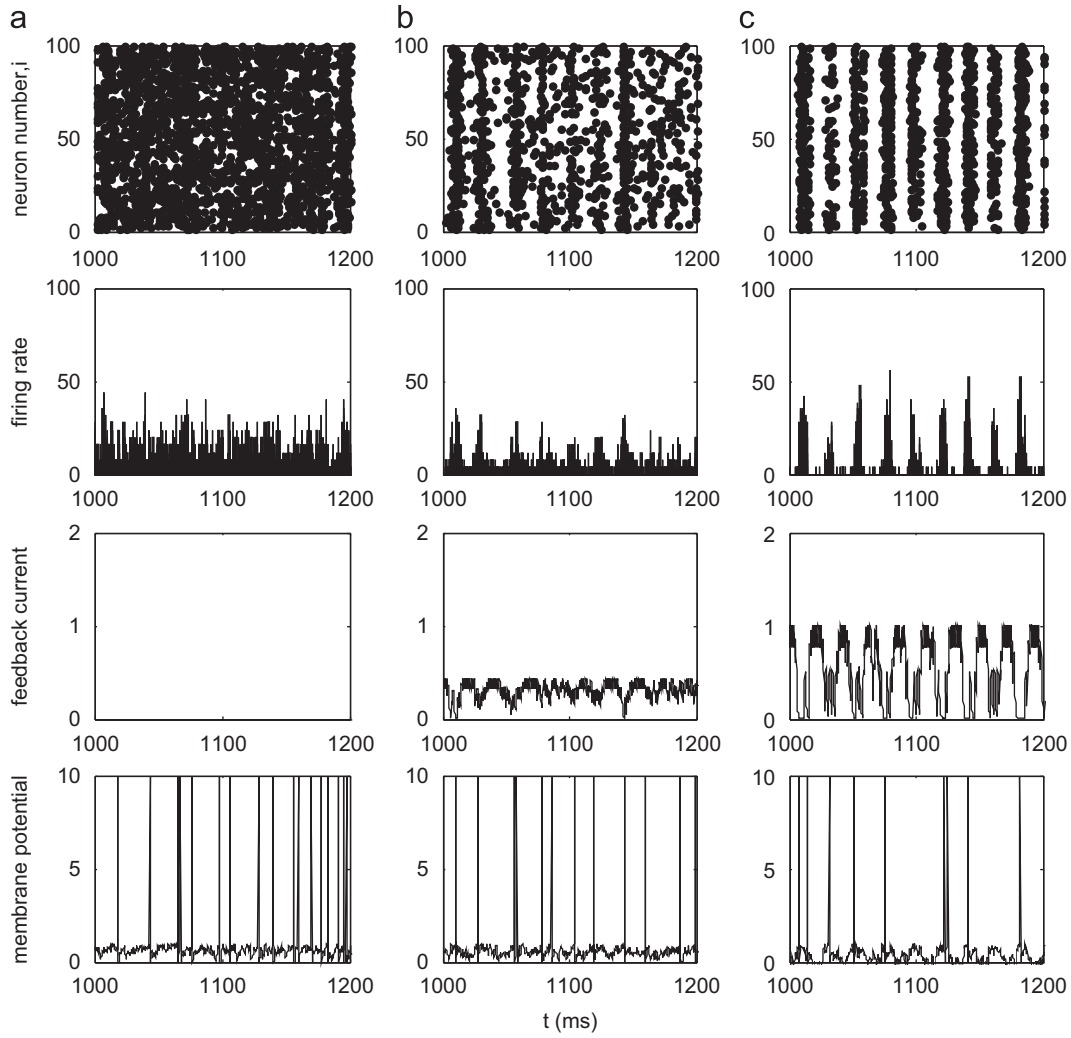

Fig. 2. Illustrations of the model behavior. Raster plots, network firing rate in spikes per second, feedback current and membrane potential (in dimensionless units) of a single neuron for (a) $G=0$, (b) $G=0.3$, and (c) $G=0.7$, for the low internal noise sub-threshold regime $\mu_E=0.9$, $D_E=0.112$. The input correlation is $c=0.6$ here and for all other figures except Fig. 11.

G in Fig. 4 (bottom) also increases monotonically, but starts to rise at a larger value of gain than in the sub-threshold case.

Moreover, *Cor* in the supra-threshold regime reaches significantly higher values than in the sub-threshold regime. Since correlation can be proportional to firing rate in feed-forward networks [7], it is likely that the increase of *Cor* with the bias μ_E is a consequence of the associated increased firing rate. To gain more insight into the increase in *Cor*, we now look at the spectral properties of the spike trains.

4. Spectral coherence and correlation

4.1. Definition of spectral coherence

To better understand the relationship between *Cor* and G, we calculate the spike train power spectrum and the mean firing rate of a single excitatory neuron in the network for different values of G. Since the statistics of spike trains are the same for all excitatory neurons, it suffices to show the firing rate and power spectrum for one neuron. The spike train power spectrum of neuron i is determined by:

$$S(\omega) = \langle \tilde{y}_i \tilde{y}_i^* \rangle \tag{12}$$

and

$$\tilde{y}_i(\omega) = \frac{1}{\sqrt{L}} \int_0^L e^{-i\omega t} y_i(t) dt, \tag{13}$$

where $\tilde{y}_i$ is the Fourier transform of the spike train, and $\tilde{y}_i^*$ denotes the complex conjugate of $\tilde{y}_i$. The brackets represent an average over multiple realizations of the external individual noise ξ_i and of the internal noise η_i, which change from trial to trial. Neglecting the temporal patterning of spikes, an arbitrary neuron i can also be simply characterized by its mean firing rate $\lambda_i = \langle y_i(t) \rangle$, where the average is taken across trials and over time.

The sub-threshold regime with small internal noise D_E is chosen to illustrate the dynamic behavior of the network with varying inhibitory feedback gain. As Fig. 5 illustrates, the spectrum of the neuron exhibits a peak at frequency in the gamma range when G is strong enough ($G > 0.2$). The appearance of the peak means the excitatory neurons are exhibiting epochs of oscillatory activity that are caused by the inhibitory feedback [8,9]. These gamma oscillations likely influence the correlations between neurons. We further find that with the increase of G, the height of the gamma peak, denoted h_p, exhibits a drastic increase from $G=0.3$ to $G=0.5$ (Fig. 5(a)–(c)), but increases only slightly beyond $G=0.6$ (Fig. 5(d)).

Author's personal copy

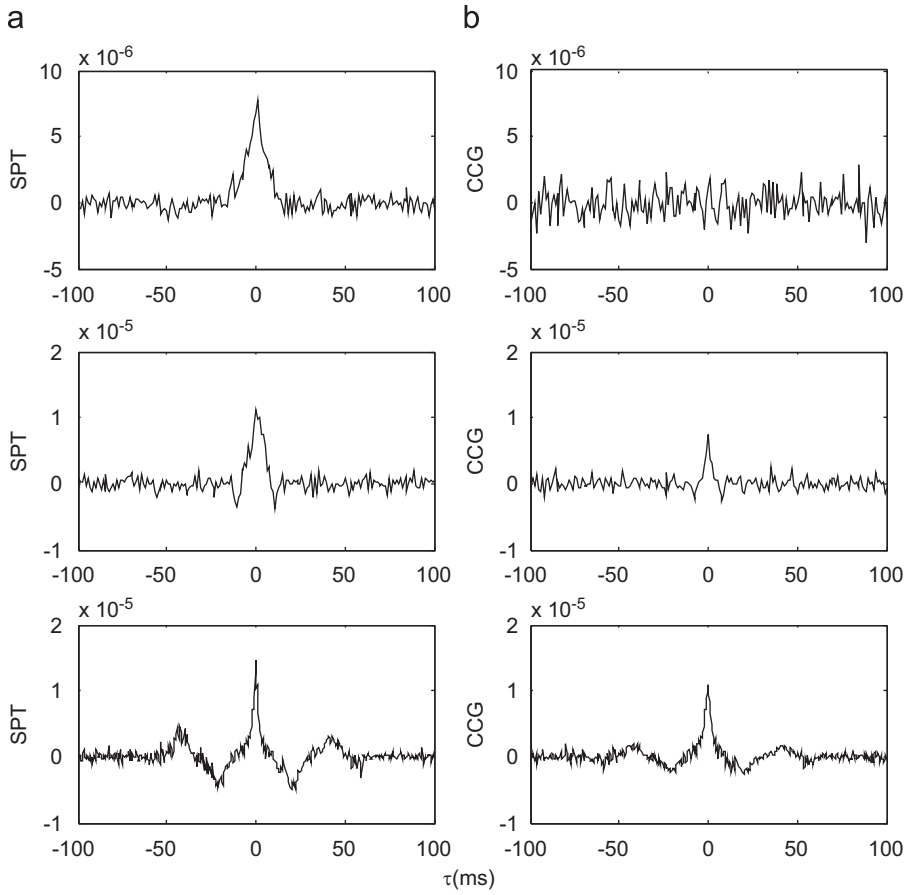

Fig. 3. Shift predictor SPT (a) and the cross-correlogram *CCG* with SPT subtracted (b) vs time lag τ. Top, $G=0$. Middle, $G=0.3$. Bottom, $G=0.7$. Simulations are done for the low internal noise sub-threshold regime $\mu_E=0.9$, $D_E=0.112$. Here the common noise ξ_c in Eq. (3) is frozen across trials. In contrast, the SPT's for the case where the common noise varies across trials are flat (not shown).

Since the power of the gamma oscillations varies with the inhibitory feedback gain, we then measure the regularity of the spike train in the frequency domain for different values of *G*. The tendency of the power spectrum to present a sharp peak can then be quantified by the degree of spectral coherence used in the stochastic dynamics literature [38,27]:

$$\beta = \frac{h_p}{\Delta\omega}\omega_p, \tag{14}$$

where h_p and $\Delta\omega$ are, respectively, the height and width-at-half-maximum of the averaged spectrum peak at frequency ω_p. This measure can then be compared with the correlation coefficient of the network.

4.2. Frozen input noise

We first consider the sub-threshold low internal noise case. *Cor*, the coherence β, and the mean firing rate *R* are plotted as a function of G, first for the low noise case (Fig. 6). Because of the inhibitory feedback, the firing rate of the neuron decreases as *G* increases (Fig. 6 middle). Further, as expected from Fig. 5, the coherence increases monotonically with *G* (Fig. 6 bottom) following a sigmoidal relation. This is the case for the sub- and suprathreshold regimes.

Our results with frozen common noise show relatively little variation in *Cor* with *G* except when *G* goes past a certain value. Fig. 6 shows that this value is $G\sim0.3$ in the sub-threshold regime at lower noise, and that β is relatively low over the same range of *G*. This suggests that, for lower *G*, any increase in *Cor* that one might expect from weak global coupling is offset by the decreasing firing rate (Fig. 6). At higher *G*, the mean rate decreases more slowly, but β shows an abrupt increase. The growth in *Cor* now parallels that of β, suggesting that *Cor* is now determined

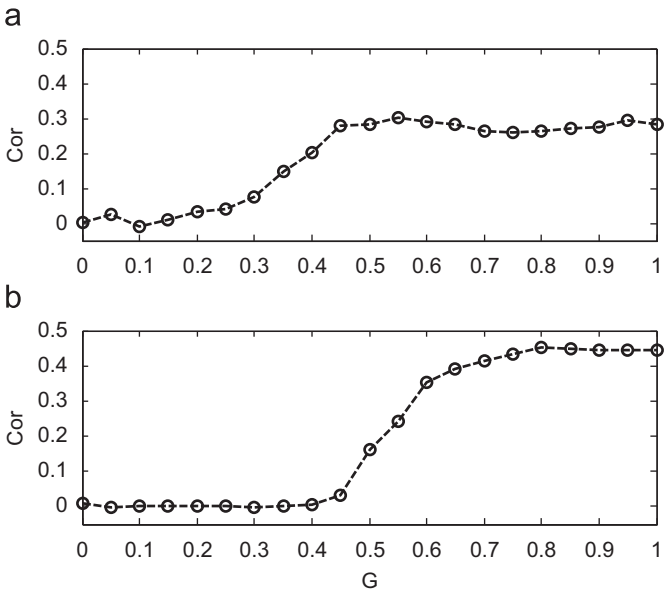

Fig. 4. Pairwise correlation coefficient (*Cor*) remains near zero, then increases with the strength of inhibitory feedback (*G*) for the low internal noise case $D_E=0.112$. (a) Sub-threshold base current with $\mu_E=0.9$. (b) Supra-threshold base current with $\mu_E=1.2$. Here the common noise ξ_c is frozen across trials. The integration window for the *CCGs* is $T=100$ ms.

Author's personal copy

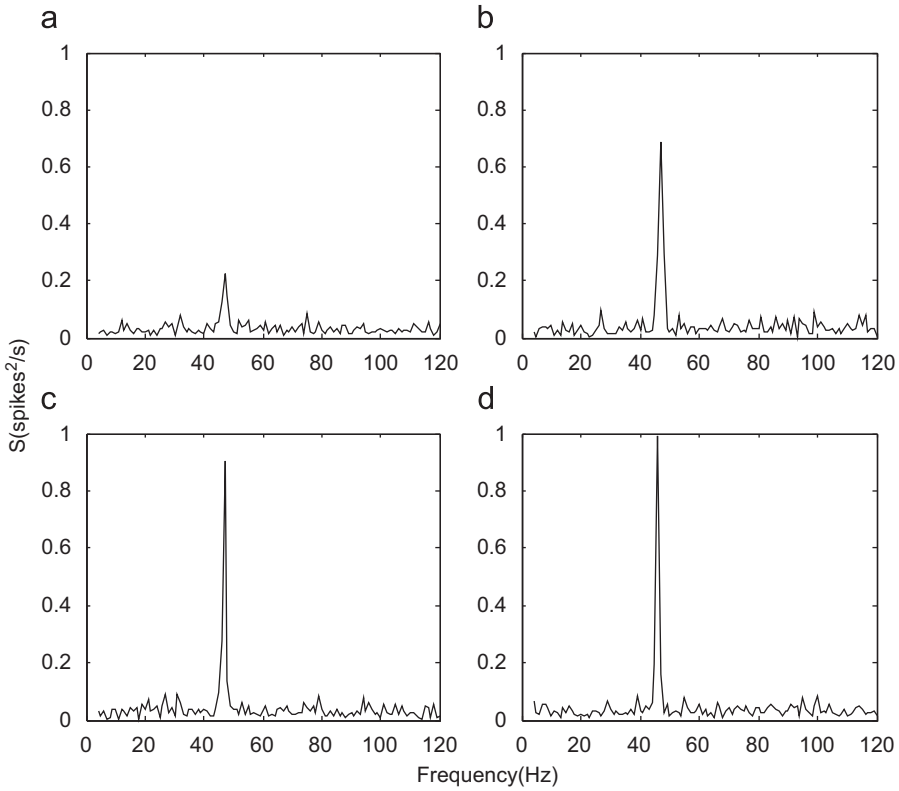

Fig. 5. Spike train power spectra at different strengths of inhibitory feedback gain G for μ_E=0.9 with low internal noise D_E=0.112. (a) G=0.3; (b) G=0.4; (c) G=0.5; (d) G=0.6. The peak corresponding to the frequency of the asynchronous oscillation increases with gain, with very little variation in frequency.

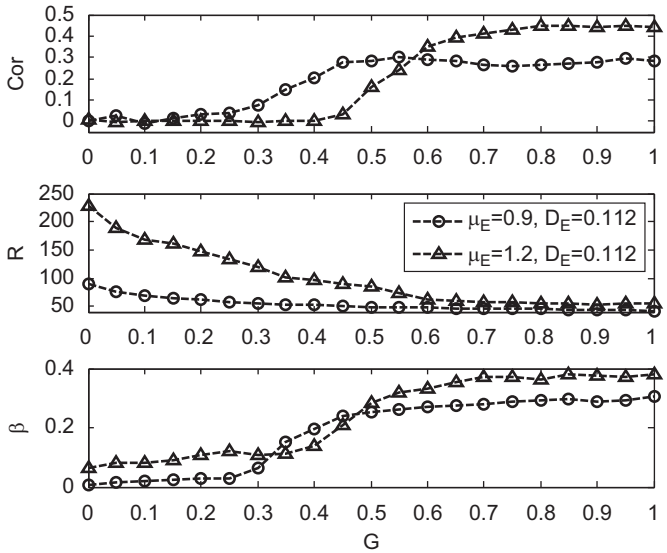

Fig. 6. Pairwise correlation coefficient (*Cor*) (top), mean firing rate (in spikes/sec) (R) (middle) and spectral coherence of spike trains (β) (bottom) as a function of feedback gain (G) in the sub-threshold regime (circles, μ_E=0.9, D_E=0.112) and supra-threshold regime (triangles μ_E=1.2, D_E=0.112). *Cor* remains near zero until moderate values of G where it starts increasing. The coherence parallels the behavior of *Cor*. The firing rate decreases with increasing G, as expected for inhibitory feedback. Here the common noise ξ_c is frozen across trials. The integration window for the *CCGs* is T=100 ms.

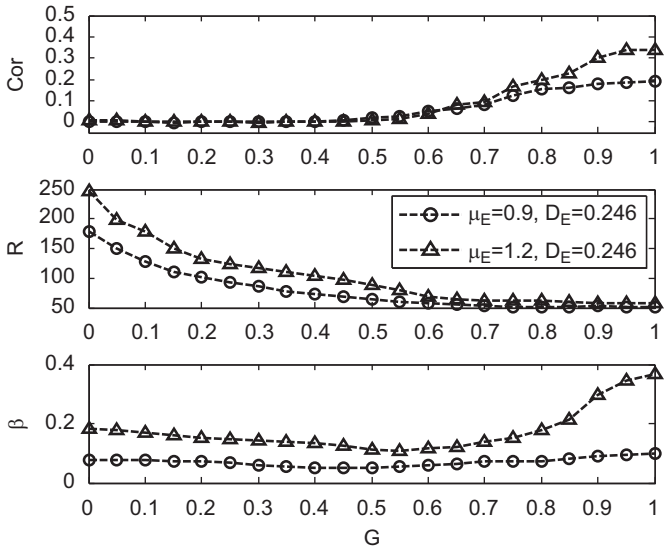

Fig. 7. Correlation coefficient (*Cor*) (top), mean firing rate (in spikes/sec) (R) (middle) and spectral coherence of spike trains (β) (bottom) as a function of feedback gain (G) for the higher noise case D_E=0.246, in the sub-threshold regime (circles, μ_E=0.9) and supra-threshold regime (triangles μ_E=1.2). Here the common noise ξ_c is frozen across trials. The behaviors are qualitatively the same as for the low noise case (Fig. 6). In the subthreshold regime, the mean rate is higher than in the low noise case. The integration window for the *CCGs* is T=100 ms.

mainly by the oscillatory strength and less by the mean rate. Fig. 7 also shows that this reasoning holds for the higher noise case, for both the sub- and suprathreshold regimes.

The magnification offered by Fig. 6 shows that *Cor* actually increases abruptly at $G\sim$0.45 for low noise (triangles). From Fig. 7, β is also lower for the sub-threshold case, but eventually increases, which suggests that the lower value of β is at least partly responsible for delaying the increase in *Cor* out to larger gains compared to the sub-threshold case. Fig. 7 shows that *Cor* with higher noise is insensitive to feedback over an even larger range of G (up to $\sim$0.6) compared to the lower noise case (Fig. 6).

Author's personal copy

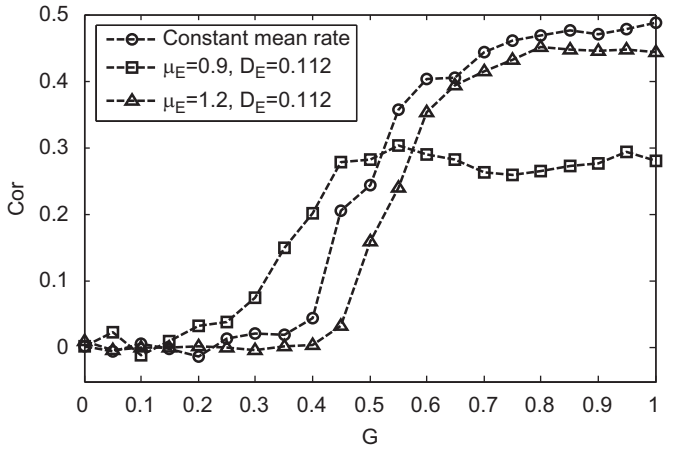

Fig. 8. Correlation coefficient (*Cor*) as a function of feedback gain (G) by maintaining the firing rate constant. Low noise is assumed throughout (D_E=0.112). The rate is controlled by increasing the bias along with G, namely using the successive values μ_E=[0.9, 0.96, 1.05, 1.1, 1.14, 1.2, 1.23, 1.28, 1.32, 1.365, 1.4, 1.435, 1.46, 1.495, 1.535, 1.56, 1.595, 1.645, 1.705, 1.757, 1.815] (circles). This controlled rate case is compared with the curves in Fig. 4 for the subthreshold (μ_E=0.9, squares) and suprathreshold (μ_E=1.2, triangles) regimes. Here the common noise ξ_c is frozen across trials. The integration window for the *CCGs* is T=100 ms.

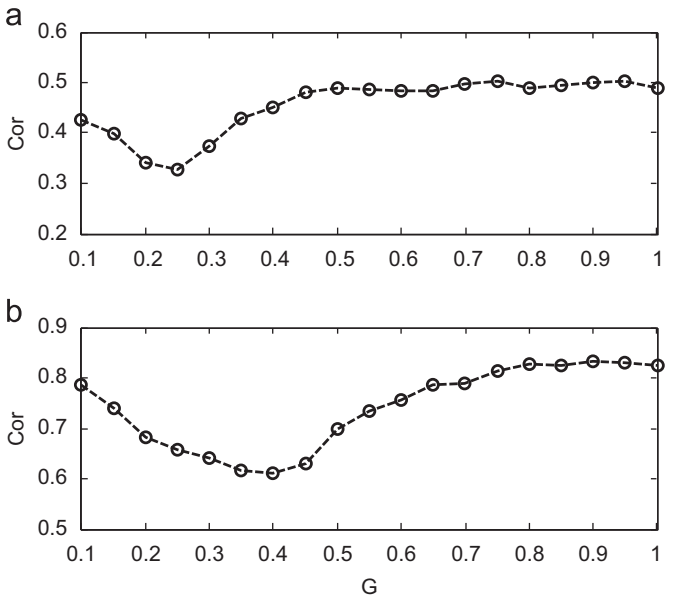

Fig. 9. Correlation coefficient (*Cor*) vs the inhibitory feedback gain (G) in the low noise regime D_E=0.112 when the common noise ξ_c in Eq. (3) is varied across trials (but is the same for each neuron in a given trial). (a) Subthreshold regime with μ_E=0.9. (b) Suprathreshold regime with μ_E=1.2. This leads to a non-monotonic dependency of *Cor* on G. The corresponding behaviors of the rate R and coherence β are the same as for the frozen common noise shown in Fig. 6 (middle and bottom panels). The integration window for the *CCGs* is T=100 ms.

At higher noise, *Cor* and β are also seen to be higher for the suprathreshold regime. Finally, Fig. 7 shows that β and *Cor* grow similarly in the higher noise case—even though β actually shows a small dip around G=0.55. So again, these results suggest that the effects of rate and coupling offset each other up to moderate values of G, and that the correlating effect of network oscillations takes over at higher G. Overall in fact, one sees a clear co-variation of *Cor* and β across regimes for frozen common noise. This will also be the case when the common noise varies across trials (Figs. 9 and 10).

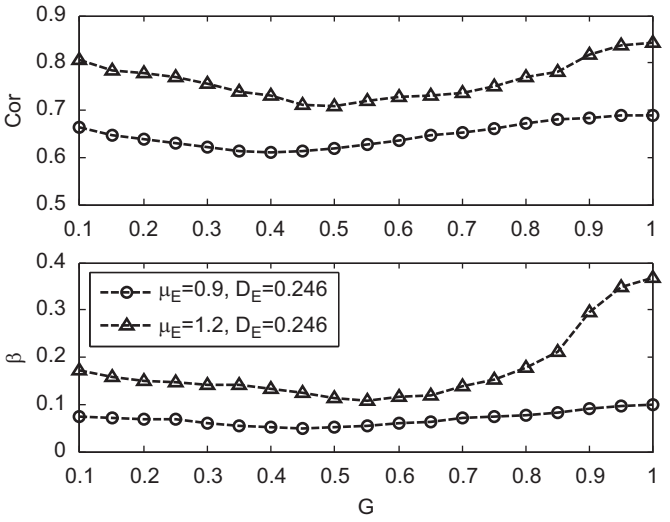

Fig. 10. Correlation coefficient (*Cor*) and spectral coherence of spike trains β for higher noise D_E=0.246 as a function of feedback gain (G) in the subthreshold (circles,μ_E=0.9) and suprathreshold regime (triangles, μ_E=1.2). Firing rates are the same as in Fig. 7. As in Fig. 9, the common noise in Eq. (3) is varied across trials, but is the same for each neuron in a given trial. The integration window for the *CCGs* is T=100 ms.

4.3. Constant firing rate simulations

To gain more insight into the relative effects of mean rate and β, we have further investigated *Cor* vs G (with frozen common noise) when the mean rate is kept approximately constant and equal to its value in open-loop. This was achieved by adjusting the bias upwards as G increased. This was done for the sub-threshold lower noise case. Fig. 8 plots *Cor* vs G and compares it to the case where the rate is allowed to decrease (Fig. 6 upper panel). *Cor* reaches higher values with the constant rate, but is maintained near zero over a slightly wider range of G values (0–0.4 instead of 0–0.25). Given that the rate is constant, one might expect that the correlating effect of the oscillation, i.e. of β (Fig. 6) be exposed for smaller values of G, and thus that *Cor* would jump up for $G<0.25$ rather than for a larger $G\sim0.4$.

However, the comparison is not so simple, because maintaining the rate constant implies that we are looking at higher biases (see the caption of Fig. 8). In particular, when G=0.25, the required bias is already 1.2, i.e. the regime has changed between the sub- and supra-threshold cases we have been studying. A more appropriate comparison may then use *Cor* vs G for the supra-threshold regime with low noise with decreasing rate (Fig. 8 triangles, from Fig. 4b). The constant rate curve jumps up earlier than the curve with decreasing rate. This supports the notion that *Cor* is no longer held low by the decreasing rate, and can thus reflect the correlations imparted by the coupling.

4.4. Common noise varies across trials

We have also performed simulations for the case where the common noise ξ_c varies across trials. Fig. 9 shows results for the low noise case, with the same low noise value used earlier. One now sees that the curve is non-monotonic for both the sub- and suprathreshold regimes. The value of *Cor* does not start at zero in open loop, as it did for frozen common noise. Further, the value of *Cor* for G=0 increases with the mean firing rate as in de La Rocha et al. [7]. This can be seen by looking at the mean firing rate for the two biases in Fig. 6 (middle panel): the higher bias of the suprathreshold case produces a higher mean rate than the subthreshold case, even though the rate decreases with gain in

Author's personal copy

both cases. The higher rate case has a value of $Cor=0.79$, in contrast to the lower rate case where it is 0.42. The *Cor* values are in fact consistently higher for the suprathreshold regime across the range of feedback gains. This implies that the system is in a regime where the output correlation is proportional to output firing rate.

Fig. 10 shows results for higher noise in the sub- and suprathreshold cases. The *Cor* vs *G* curve is again non-monotonic, with a minimum around $G=0.45$. This contrasts with the minimum around $G=0.3$ for low noise (Fig. 9). In both cases the drop in correlation at low *G* mirrors the drop in firing rate (Fig. 6 middle panel). Further, Fig. 10 shows that the increase in correlation seen at higher *G* likewise parallels the increase in β. Thus, the co-variations in rate and β in this case suggest that the shape of *Cor* vs *G* is again determined by an interplay of dropping mean rate and an increasing network oscillation. A fuller understanding will require more theoretical and computational work beyond the scope of this paper.

It is important to note that we have investigated two different sets of simulations, corresponding to two types of stimulation: across trials, the common noise is (1) constant or (2) varied. These two kinds of stimulation can also be implemented experimentally. In both cases, one has to correct for SPT. Our point here is that, depending on how one does the experiment or simulation, one will get a different view of how correlations vary with feedback gain. The non-SPT corrected correlogram data in the frozen noise case are non-monotonic, and have higher values than the SPT-corrected ones for all gain values (not shown). The SPT correction thus removes the common noise-induced correlations in the firing rates of the cells. When the common noise varies across trials, the SPTs are flat (not shown); then their subtraction from the *CCG* does not alter the shape of the *CCG*, yielding overall larger areas under the curve and consequently larger values of *Cor*.

All the results up to now regarding the dependence of *Cor* on *G*, whether the frozen noise was varied or not, were obtained for the relatively high input correlation $c=0.6$. However, it is known that the transfer of input correlations to output correlations (i.e. the correlation susceptibility) is more significant for weaker input correlations [45]. We thus tested whether the results were qualitatively the same for lower input correlations. Fig. 11 shows the results for varying common noise in the case $c=0.2$. Again a non-monotonic behavior is seen as in Fig. 9 (top), and in fact the minimum occurs at about the same value of gain. The same story holds with frozen common noise (not shown). While we have not explored the full range of c values, such as very strong or very weak ones, these results suggest that the feedback dependence of *Cor* is a robust phenomenon for a good range of input correlations. The foregoing results also show that the system is in parameter regimes where output correlation is proportional to input correlation and firing rate.

5. Heterogeneous network

Up to this point we have not taken into account the heterogeneity of the network. As shown by previous studies, heterogeneity can desynchronize networks ([3,48]), because it can translate into variability in intrinsic action potential frequency, which weakens correlations in the network. Also, threshold (or bias) heterogeneity can increase firing in the presence of recurrent excitation, because the more excitable cells can help recruit others. Here we briefly study the effect of the heterogeneity on the relationship between *Cor* and *G* with global inhibition, since this inhibition affects the rate and oscillation regularity. We achieve this goal by distributing either *G* or the firing threshold v_T for each cell according to Gaussian statistics. These are parameters that are likely to vary significantly across cells since, for example in the electrosensory system (see [6] and references therein) the different excitatory cells have a distribution of firing rates, and the feedback synapses are not identical and furthermore can be plastic.

Fig. 12 shows the results of computer simulations for the correlation coefficient of the network with delayed inhibitory feedback described in Fig. 1, when either *G* (triangles) or v_T

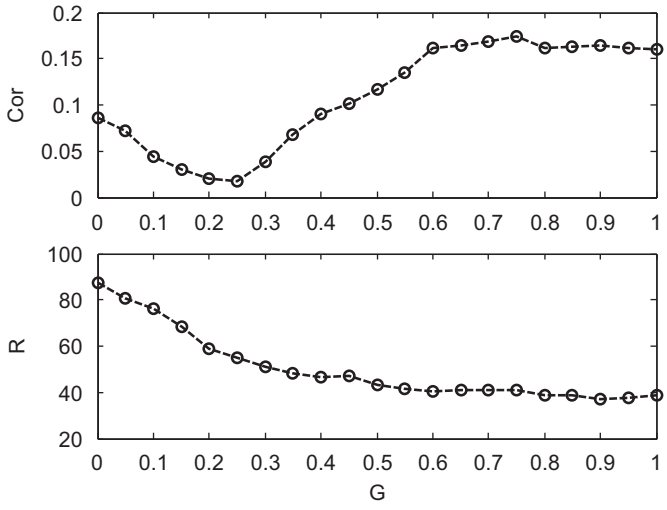

Fig. 11. Correlation coefficient (*Cor*) (top) and mean firing rate (bottom) vs the inhibitory feedback gain (*G*) for a lower strength of the input correlation, $c=0.2$. Parameters are for the subthreshold low noise regime as in Fig. 9 (top), i.e. $\mu_E=0.9$, $D_E=0.112$. The common noise in Eq. (3) is varied across trials, but is the same for each neuron in a given trial. The non-monotonic behavior is still seen as in the $c=0.6$ case, but the *Cor* values are lower. The integration window for the *CCGs* is $T=100$ ms.

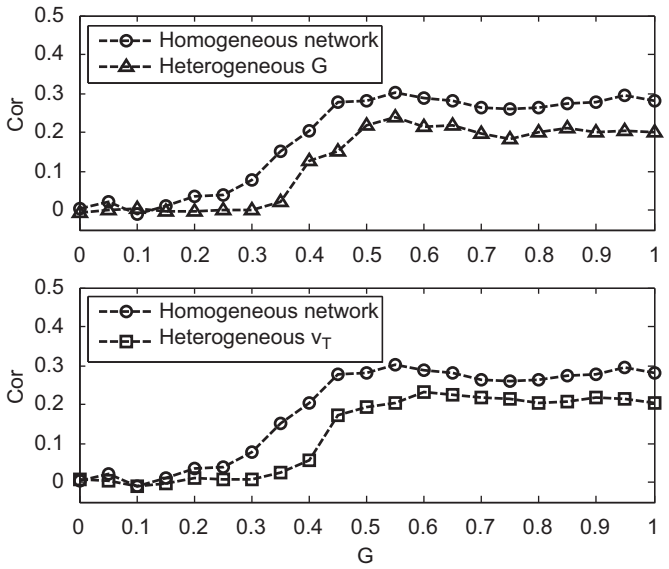

Fig. 12. A heterogeneous network is compared to a homogeneous one for frozen common noise in the low noise subthreshold regime ($\mu_E=0.9$, $D_E=0.112$). Curves with circles represent the correlation coefficient *Cor* vs feedback gain *G* when the network is homogeneous. (a) Values of *G* are static in time but Gaussian-distributed across the neurons (triangles). (b) The spiking threshold v_T is Gaussian distributed (squares). In either case the standard deviation of the parameter distribution is $\sigma_E=0.03$. The integration window for the *CCGs* is $T=100$ ms. Heterogeneity decreases *Cor*, yet preserves its qualitative dependence on *G*.

Author's personal copy

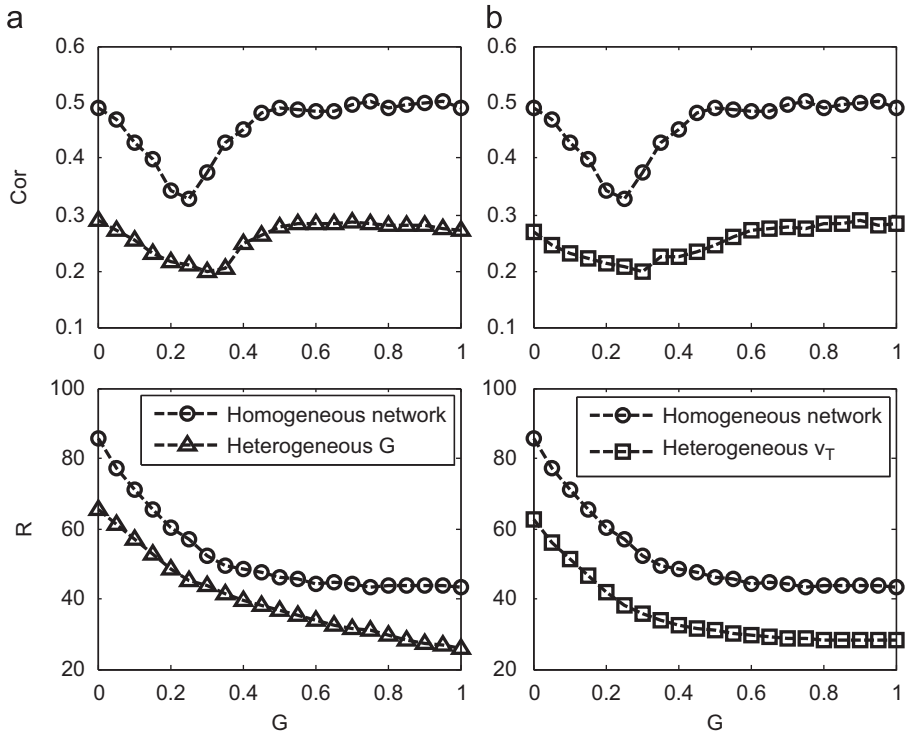

Fig. 13. Effect of heterogeneity on the correlation coefficient (*Cor*) and mean rate (*R*) for common noise that varies across trials. Left panels are for noise on *G*, while the right panels are for noise on the spiking threshold v_T. All parameters are as in Fig. 12. The integration window for the *CCGs* is $T=100$ ms.

(squares) is Gaussian-distributed. Such static Gaussian parameter noise alters the values of *Cor* and *R* when other parameters remain the same. The increase in *G* results in a similar decrease in mean rate *R* for both cases (heterogeneous *G* or heterogeneous v_T), but *R* vs *G* is shifted down to values about 20–25% lower in the heterogeneous case compared to the homogeneous case (Fig. 13 lower panels). While we do not explore this effect in detail (which would require theory), intuitively the cells closer to threshold fire more readily and produce more inhibition. Likewise the pathways with more gain produce more inhibition. In both cases the mean rate is lowered. This contrasts with excitatory feedback, where heterogeneity leads to more firing as the more excitable cells recruit the other cells.

The disordering effect of the heterogeneity also results in lower values of *Cor* compared to the homogeneous case. However, in spite of this moderate amount of heterogeneity, the same shape is seen in the *Cor* vs *G* curve. This is also the case for non-monotonic relationship between *Cor* and *G* in the case where the common noise is varied across trials (Fig. 13). Thus the shape of the *Cor* vs *G* characteristic is robust to low-variance static parameter noise. In summary, with respect to output pairwise correlations in this system with global inhibition, there are no qualitatively unique effects that arise from heterogeneity of the gain and distance-to-threshold.

6. Discussion and outlook

We have shown that the relationship between the network-averaged pairwise correlation coefficient (*Cor*) of firing rates and the strength of the global inhibition in that network is monotonic increasing for frozen common noise. Our results in Figs. 4, 6–8 reveal that the correlation remains near zero starting from zero gain (open-loop, i.e. feedforward case) up to moderate gains. This implies that factors affecting feedback strength will have little impact on the correlation at lower gains. However, as the gain increases beyond moderate values, the correlation increases quite rapidly, especially when the internal noise is lower. Our results suggest that this increase in *Cor* is associated with the emergence of oscillatory activity, which is in the gamma frequency range for the parameters of interest derived from the electric sense. Thus, *Cor* signals the emergence of network oscillations in networks with global inhibitory feedback.

Our results with common noise that varies across trials (Figs. 9–11 and 13) start at a non-zero value proportional to the bias (and thus the firing rate). They show an initial decrease of *Cor* with *G*, but qualitatively the same behavior as with frozen noise for larger *G*. In that case also the emergence of a network oscillation is associated with the increase in *Cor*. Thus, in both the frozen and varying common noise cases, and for the four regimes we have studied (low and high noise, sub- and supra-threshold), the increase in peak coherence β for moderate to high values of *G* is a good indicator of the behavior of the pairwise correlation. As discussed in Section 4.4, the correlation differences between the two stimulation scenarios arise from the different shape of the SPTs, combined with the behavior of the shape and area under the cross-correlogram as the gain changes (Fig. 3).

The quantity *Cor* is expected to decrease as the mean rate decreases if the correlations are not too strong [7,45]. The results of Fig. 6 along with those in Section 4.4 show that our system operates in similar regimes (although with feedback), since *Cor* is proportional to input correlation and to the mean firing rate (the latter being increased by increasing the bias). This is the case both for feedforward ($G=0$) and for all feedback gains investigated. But the inhibition causes the rate to decrease in proportion to its strength. While we lack a full theory for these phenomena (see below), our results suggest that this decrease is partly responsible for maintaining *Cor* near zero at lower gains (or to decrease *Cor* with varying common noise). This picture is further

Author's personal copy

supported by simulations in which G is increased concomitantly with bias to maintain a constant rate. Eventually at higher gains the network oscillation has a more important effect on *Cor*.

Our model is inspired by earlier experimental work on the electrosensory system [8,9], in which the internal and external noises were band-limited (i.e. colored). Early modeling in [8] used only one colored Ornstein–Uhlenbeck noise source, that drove either a single or all neurons. In the model of Doiron et al. [9], the noises were made Gaussian and white to simplify the theory. The full theory developed in Lindner et al. [28] again used the Gaussian white noise approximation. Our computational model here uses colored external noises and Gaussian white internal noise, because the bandwidth of the external noises associated with stimuli is smaller than that of voltage fluctuations. Further, the inhibitory feedback from the principle (excitatory) cells to each other in reality involves another nucleus (nP) whose cells provide the inhibition. This was simplified in Doiron et al. [8,9] and Lindner et al. [28] by assuming the cells inhibited each other directly. Here, as in Marinazzo et al. [31], we have modeled an inhibitory neuron from nucleus nP. This also prevents a direct application of the theory in Lindner et al. [28]. Nevertheless, that theory can be developed further to include the inhibitory neuron. As this neuron has internal noise (Eq. (6)) that linearizes its response, linear response theory could be applied to it. The external noises could also be given equivalent white noise intensities. Alternately one could redo simulations directly for the model in Lindner et al. [28]. In both cases, one would have to extend the theory to compute the correlations as in [7] (Supplementary Material), but with feedback input as an extra "small" input. Also the theoretical cross-spectra in Lindner et al. could be integrated numerically to provide correlation information.

The structure of our model enables us to predict that the results will not be sensitive to whether the individual noise in the cells originates internally or externally to the sensory system. The pairwise correlation effects reported here will also be induced by the global inhibitory feedback component of a more general recurrent network. It may be obscured by correlations caused by other feedback loops of different polarities and spatial structure.

The monotonic *Cor* vs G curves for frozen common noise, or their non-monotonic version for varying common noise, are robust over a range of noise intensities and biases, but also when the network is heterogeneous with $\pm 3\%$ parameter variations around their nominal values. Gaussian-distributed firing thresholds or feedback gains yield moderately smaller correlation values, but the curve shape is preserved. We note that the increased noise caused by the heterogeneity moves the point at which *Cor* jumps up to higher values of G. This is also the case when the internal dynamical noise intensity is increased (compare Figs. 6 and 7), which makes sense intuitively.

Our simulations reveal that there are subtle effects at work in this network. For example, the coherence β exhibits the aforementioned small dip for $G \sim 0.55$ (Figs. 7 and 10). Moderate feedback gain slightly suppresses the oscillation for higher noise, due to its effect on the three components that go into the computation of the coherence; the origin of this effect is not known at this time. Also, if one compares the sub-threshold regime at lower (Fig. 6) and higher (Fig. 7) noise, one sees that the noise has slightly increased the strength of the network oscillation at lower gains. This appears to be an example of a noise-induced oscillation, which is a form of coherence resonance ([29,38] and [27,35]). This is often the case for systems near the threshold of a Hopf bifurcation. More work is needed to pinpoint the precise origin of this effect here. The potential existence of these subtle effects partly motivated our investigation of the sub- and suprathreshold regimes with low and high noise.

More work is thus needed to disentangle the various effects of the model parameters on *Cor*. For example, without a thorough analysis (beyond the scope of our work), it is hard to argue that β is also higher for the constant rate curve in Fig. 8 than for the decreasing rate curve, without knowing how it varies as a function of bias and gain along the curve—and how all this depends on noise level. As the bias increases, the cells behave more deterministically. Our simulations reveal that this subtly affects β; in particular, the noise floor increases with bias, which confounds measures of oscillation strength. The theory in Lindner et al. [28] has not been explored in detail with respect to the dependence of oscillation strength (peak height or spectral coherence) on bias, gain and noise. Constant rate simulations as reported in Fig. 8 partially clarify the origin of the *Cor* vs G dependency, but the fuller story will have to wait more theoretical/numerical studies.

Throughout our work, we have considered how the pairwise correlation covaries with the mean rate. In particular, when the common noise varies across trials, the drop in rate accompanies the drop in correlation. Oscillations then grow as gain increases in spite of the further drop in rate. We have also shown in Section 4.4 that our system, at lower gains, output correlation grows with mean rate as in de La Rocha et al. [7]. While we do not have a theory for the numerical effects we report, our results suggest that correlation results in part from the interplay between rate and oscillation. It remains to be seen how this interplay plays out in other connection topologies. Delayed feedback dynamics via local inhibitory coupling also show oscillations ([17,20]), and thus qualitatively the same behaviors may occur in that case. In certain systems, the strength of correlations has been shown to be inversely proportional to the distance between neurons [24,43]. The effects seen here may be altered by such an inverse law. Also, while our study has focused on inhibitory feedback, excitatory feedback present in certain systems will also play a correlating role. Preliminary results with our network indeed reveal that the pairwise correlation simply increases monotonically with the strength of excitatory feedback (not shown); the system however saturates to a high firing state if this feedback is too strong. It will be interesting to explore the scenario where both feedback polarities are present as is known to occur in the electric sense, and whether this leads to low correlations [11].

In our study we have used a long time window to integrate the correlation over a large range of time lags (Eq. (10)). Such a large window leads to a measure of the correlation in the firing rates on longer time scales, which has been the focus of our work. If a small time window is used, the pairwise correlation then becomes more a measure of synchrony. It is known that the pairwise correlation increases with the time window T and eventually saturates ([7] Supplementary Material; [22]). We have verified that this is the case for our data as well (not shown). Further, the oscillations in the *CCG* at higher gains (Fig. 3) will produce a correlation value that oscillates with T on top of an overall increase in *Cor* (not shown), because the integration of the *CCG* (Eq. (10)) will end at a different part of the (damped) oscillation cycle as T varies. Overall however, the dependence of correlation on feedback gain is not expected to change qualitatively for a range of T values. They may change at very short T's. In particular, Lindner et al. [28] showed that there are differences between cross-correlation and autocorrelation on fast time scales for a similar system (but not beyond).

Also, several studies reveal that correlations often depend in complex ways on network connectivity [15,37,45], filtering caused by synapses and membranes [46] and the details of the spike generating model [37,21,47]. For the pyramidal cells within the electrosensory lateral line lobe, the correlations also depend on the amount of receptive field overlap [6], with cell pairs

Author's personal copy

sharing little receptor afferent input showing negligible correlated activity. Finally, we have kept the input correlation fixed at 0.6 throughout, except for Fig. 11 where we illustrate the effect of a lower input correlation of 0.2. This revealed an overall lower output correlation, but the same non-monotonic shape when the common noise varied across trials. Correlations were also lower and depended monotonically on gain for the frozen common noise case (not shown). Very low or very high strengths of these common fluctuations may influence the results shown here [21,45].

Acknowledgments

The authors thank Jérémie Lefebvre and Alexandre Payeur for technical computing assistance. This work was supported by the National Natural Science Foundation of China under grant no. 61075105 to ZJW, by a China Scholarship Council award to XJL and by the Natural Sciences and Engineering Council of Canada under grant no. 121891-2009 to AL.

References

[1] D. Amit, N. Brunel, Model of global spontaneous activity and local structured activity during delay periods in the cerebral cortex, Cereb. Cortes 7 (1997) 237–252.
[2] W. Bair, E. Zohary, W.T. Newsome, Correlated firing in macaque visual area MT: time scales and relationship to behavior, J. Neurosci. 21 (2001) 1676–1697.
[3] M. Bartos, I. Vida, P. Jonas, Synaptic mechanisms of synchronized gamma oscillations in inhibitory interneurons networks, Nat. Rev. Neurosci. 8 (2007) 45–56.
[4] C. Borgers, N. Kopell, Synchronization in networks of excitatory and inhibitory neurons with sparse, random connectivit, Neural Comput. 15 (2003) 509–538.
[5] N. Brunel, X.J. Wang, What determines the frequency of fast network oscillations with irregular neural discharges? I. synaptic dynamics and excitation-inhibition balance, J. Neurophysiol. 90 (2003) 415–430.
[6] M.J. Chacron, J. Bastian, Population coding by electrosensory neurons, J. Neurophysiol. 99 (2008) 1825–1835.
[7] J. de La Rocha, B. Doiron, E. Shea-Brown, K. Josic, A. Reyes, Correlation between neural spike trains increases with firing rate, Nature 448 (2007) 802–806.
[8] B. Doiron, M.J. Chacron, L. Maler, A. Longtin, J. Bastian, Inhibitory feedback required for network oscillatory responses to communication but not prey stimuli, Nature 421 (2003) 539–543.
[9] B. Doiron, B. Lindner, A. Longtin, L. Maler, J. Bastian, Oscillatory activity in electrosensory neurons increases with the spatial correlation of the stochastic input stimulus, Phys. Rev. Lett. 93 (2004) 048101.
[10] Y. Dong, S. Mihalas, F. Qiu, R. von der Heydt, E. Niebur, Synchrony and the binding problem in macaque visual cortex, J. Vision 8 (2008) 1–16.
[11] A.S. Ecker, P. Berens, G.A. Keliris, M. Bethge, N.K. Logothetis, A.S. Tolias, Decorrelated neuronal firing in cortical microcircuits, Science 327 (2010) 584–587.
[12] E. Edwards, M. Soltani, L.Y. Deouell, M.S. Berger, R.T. Knight, High gamma activity in response to deviant auditory stimuli recorded directly from human cortex, J. Neurophysiol. 94 (2005) 4269–4280.
[13] G.B. Ermentrout, R.F. Galan, N.N. Urban, Reliability, synchrony and noise, Trends Neurosci. 31 (2008) 428–434.
[14] R.F. Galan, N. Fourcaud-Trocme, G.B. Ermentrout, N.N. Urban, Correlation-induced synchronization of oscillations in olfactory bulb neurons, J. Neurosci. 26 (2006) 3646–3655.
[15] I. Ginzburg, H. Sompolinsky, Theory of correlations in stochastic neural networks, Phys. Rev. E. 50 (1994) 3171–3190.
[16] D.A. Gutnisky, V. Dragoi, Adaptive coding of visual information in neural populations, Nature 452 (2008) 220–224.
[17] D. Hansel, H. Sompolinsky, Chaos and synchrony in a model of a hypercolumn in visual cortex, J. Comput. Neurosci. 3 (1996) 7–34.
[18] A. Hasenstaub, Y. Shu, B. Haider, U. Kraushaar, A. Duque, D.A. McCormick, Inhibitory postsynaptic potentials carry synchronized frequency information in active cortical networks, Neuron 47 (2005) 423–435.
[19] J. Hertz, Cross-correlations in high-conductance states of a model cortical network, Neural Comp 22 (2010) 427–447.
[20] A. Hutt, C. Sutherland, A. Longtin, Driving neural oscillations with correlated spatial input and topographic feedback, Phys. Rev. E 78 (2008) 021911.
[21] K. Josic, E. Shea-Brown, B. Doiron, J. de la Rocha, Stimulus-dependent correlations and population codes, Neural Comput. 21 (2009) 2774–2804.
[22] R.E. Kass, V. Ventura, Spike count correlation increases with length of time interval in the presence of trial-to-trial variation, Neural Comp. 18 (2006) 2583–2591.
[23] K. Kitano, T. Fukai, Variability vs. synchronicity of neuronal activity in local cortical network models with different wiring topologies, J. Comput. Neurosci. 23 (2007) 237–250.
[24] A. Kohn, M.A. Smith, Stimulus dependence of neuronal correlation in primary visual cortex of the macaque, J. Neurosci. 25 (2005) 3661–3673.
[25] B. Kriener, T. Tetzlaff, A. Aertsen, M. Diesmann, S. Rotter, Correlations and population dynamics in cortical networks, Neural Comput. 20 (2008) 2185–2226.
[26] B. Kriener, M. Helias, A. Aertsen, S. Rotter, Correlations in spiking neuronal networks with distance dependent connections, J Comput Neurosci. 27 (2009) 177–200.
[27] B. Lindner, L. Schimansky-Geier, A. Longtin, Maximizing spike train coherence or incoherence in the leaky integrate-and-fire model, Phys. Rev. E. 66 (2002) 031916.
[28] B. Lindner, B. Doiron, A. Longtin, Theory of oscillatory firing induced by spatially correlated noise and delayed inhibitory feedback, Phys. Rev. E. 72 (2005) 061919.
[29] A. Longtin, J.G. Milton, J.E. Bos, M.C. Mackey, Noise and critical behavior of the pupil light reflex at oscillation onset, Phys. Rev. A 41 (1990) 6992–7005.
[30] W.W. Lytton, T.J. Sejnowski, Simulations of cortical pyramidal neurons synchronized by inhibitory interneurons, J. Neurophysiol. 66 (1991) 1059–1079.
[31] D. Marinazzo, H.J. Kappen, S.C.A.M. Gielen, Input-driven oscillations in networks with excitatory and inhibitory neurons with dynamic synapses, Neural Comput. 19 (2007) 1739–1765.
[32] N. Masuda, B. Doiron, Gamma oscillations of spiking neural populations enhance signal discrimination, PLoS Comput Biol. 3 (2007) e236.
[33] A. Mazzoni, S. Panzeri, N.K. Logothetis, N. Brunel, Encoding of naturalistic stimuli by local field potential spectra in networks of excitatory and inhibitory neurons, PLoS Comput Biol. 4 (12) (2008) e1000239.
[34] K.J. Miller, E.C. Leuthardt, G. Schalk, R.P. Rao, N.R. Anderson, D.W. Moran, J.W. Miller, J.G. Ojemann, Spectral changes in cortical surface potentials during motor movement, J. Neurosci. 27 (2007) 2424–2432.
[35] R. Morse, A. Longtin, Coherence and stochastic resonance in threshold crossing detectors with delayed feedback, Phys. Lett. A 359 (2006) 640–646.
[36] G.J. Murphy, F. Rieke, Signals and noise in an inhibitory interneuron diverge to control activity in nearby retinal ganglion cells, Nat. Neurosci. 11 (2008) 318–326.
[37] S. Ostojic, N. Brunel, V. Hakim, How connectivity background activity and synaptic properties shape the cross correlation between spike trains, J. Neurophysiol. 29 (2009) 10234–10253.
[38] K. Pakdaman, S. Tanabe, T. Shimokawa, Coherence resonance and discharge time reliability in neurons and neuronal models, Neural Networks 14 (2001) 895–905.
[39] G. Palm, A. Aertsen, G. Gerstein, On the significance of correlations among neuronal spike trains, Biol. Cybern. 59 (1988) 1–11.
[40] S. Ray, E. Niebur, S.S. Hsiao, A. Sinai, N.E. Crone, High-frequency gamma activity(80–150 Hz) is increased in human cortex during selective attention, Clin. Neurophysiol. 119 (2008) 116–133.
[41] A. Renart, J. de la Rocha, P. Bartho, L. Hollender, N. Parga, A. Reyes, K.D. Harris, The asynchronous state in cortical circuits, Science 327 (2010) 587–590.
[42] E. Shea-Brown, K. Josić, J. de la Rocha, B. Doiron, Correlation and synchrony transfer in integrate-and-fire neurons: basic properties and consequences for coding, Phys. Rev. Lett. 100 (2008) 108102.
[43] M.A. Smith, A. Kohn, Spatial and temporal scales of neuronal correlation in primary visual cortex, J. Neurosci. 28 (2008) 12591–12603.
[44] T. Tchumatchenko, T. Geisel, M. Volgushev, F. Wolf, Signatures of synchrony in pairwise count correlations, Front. Comput. Neurosci. 4 (2010) 1.
[45] T. Tchumatchenko, A. Malyshev, T. Geisel, M. Volgushev, F. Wolf, Correlations and synchrony in threshold neuron models, Phys. Rev. Lett. 104 (2010) 058102.
[46] T. Tetzlaff, S. Rotter, E. Stark, M. Abeles, A. Aertsen, M. Diesmann, Dependence of neuronal correlations on filter characteristics and marginal spike train statistics, Neural Comput. 20 (2008) 2133–2184.
[47] R.D. Vilela, B. Lindner, Comparative study of different integrate-and-fire neurons: Spontaneous activity, dynamical response, and stimulus-induced correlations, Phys. Rev. E. 80 (2009) 031909.
[48] X.J. Wang, G. Buzsaki, Gamma oscillation by synaptic inhibition in a hippocampal interneuronal network model, J. Neurosci. 16 (1996) 6402–6413.

Jinli Xie, born in 1983, earned her B.S. degree in automation engineering from Shandong Polytechnic University in 2006. She is currently a Ph.D. candidate in Control Theory and Engineering, Donghua University, Shanghai, China. From 2009 to 2010, she had been a visiting researcher in Physics Department, University of Ottawa. Her research interests include computational neuroscience and neural dynamics.

Author's personal copy

Zhijie Wang was born in ZheJiang, China, in 1969. He received his Bachelor, Master, and Doctor degrees in electrical engineering from Donghua University, Shanghai, China, in 1991, 1994 and 1997, respectively. From 2000 to 2002, he was a visiting researcher in Aihara Laboratory, Department of Mathematical Engineering, The University of Tokyo. He is currently a professor at College of Information Science and Technology, Donghua University. His research interests include neural networks, fuzzy logic, and intelligent systems.

André Longtin is Professor of Physics at the University of Ottawa, where he is also cross-appointed to the Departments of Cellular and Molecular Medicine and of Mathematics and Statistics. He directs the Center for Neural Dynamics, and heads the Neurophysics and Nonlinear Dynamics Group. He received a B.Sc. Physics in 1983 and M.Sc. Physics in 1985 from the Université de Montréal, and a Ph.D. in Physics from McGill University in 1989. He joined Los Alamos National Laboratory for two years, holding a joint position in the Complex Systems Group T13 and the Center for Nonlinear Studies. He became assistant professor in 1992, and is Professor since 2002. He is a Fellow of the American Physical Society.